JOURNAL OF MATERIALS SCIENCE **39** (2004) 679–681

Transmission spectra investigation on tunable bandgap of liquid crystal infiltrated photonic crystal

DI XU, GUIGUANG XIONG
Department of Physics, Wuhan University, Wuhan 430072, People's Republic of China
E-mail: ggxiong@whu.edu.cn

Photonic bandgap (PBG) material can prohibit the propagation of light in certain directions for certain bands of frequencies along with periodic constant variations [1–3]. Appropriately, recent studies [4] bring forwards theoretical analysis involving the infiltration of liquid crystal (LC) into high index-contrast photonic crystal (PC) template. Subsequent experimental studies of temperature variation in LC/PCs confirm expected frequency-shifts of the bandgap and the reduction of peak reflection-efficiencies. Using the temperature index of a nematic liquid crystal, the 3D LC/PC [5], 2D LC/PC possessing a triangular lattice of air poles [6] and 2D LC/metallic PC [7] have been reported.

In this paper, we extend the exact formalism of finite-difference time-domain (FDTD) method of square lattice PBG structure to LC/PC structure. A well-known, efficient implementation is based on Yee's mesh [8], where the electric and magnetic field components are evaluated at different grids having the same pitch, but which have been shifted over half a grid spacing, both in space and in time. For a linear material in a source-free region, the time-dependent Maxwell's equations can be written in the following form,

$$\nabla \times \vec{E}(\vec{r}, t) = -\frac{\mu(r)\partial \vec{H}(\vec{r}, t)}{\partial t} \tag{1}$$

$$\nabla \times \vec{H}(\vec{r}, t) = \frac{\varepsilon(r)\partial \vec{E}(\vec{r}, t)}{\partial t} \tag{2}$$

where $\varepsilon(r)$, and $\mu(r)$ are the position dependent permittivity and permeability conductivity of the material, respectively. The following FDTD time stepping formulas are the spatial and time discretizations of above equations on a discrete two-dimensional mesh within the x-y coordinate system for the E polarization,

$$E_{\mathrm{z}}^{\mathrm{n}+1}(i, j) = E_{\mathrm{z}}^{\mathrm{n}}(i, j) - \frac{H_{\mathrm{x}}^{\mathrm{n}+\frac{1}{2}}\left(i, j+\frac{1}{2}\right) - H_{\mathrm{x}}^{\mathrm{n}+\frac{1}{2}}\left(i, j-\frac{1}{2}\right)}{\Delta y}\frac{\Delta t}{\varepsilon(i, j)} + \frac{H_{\mathrm{y}}^{\mathrm{n}+\frac{1}{2}}\left(i+\frac{1}{2}, j\right) - H_{\mathrm{y}}^{\mathrm{n}+\frac{1}{2}}\left(i-\frac{1}{2}, j\right)}{\Delta x}\frac{\Delta t}{\varepsilon(i, j)} \tag{3}$$

$$H_{\mathrm{x}}^{\mathrm{n}+\frac{1}{2}} = H_{\mathrm{x}}^{\mathrm{n}-\frac{1}{2}}(i, j) - \frac{E_{\mathrm{z}}^{\mathrm{n}}\left(i, j+\frac{1}{2}\right) - E_{\mathrm{z}}^{\mathrm{n}}\left(i, j-\frac{1}{2}\right)}{\Delta x}\frac{\Delta t}{\mu} \tag{4}$$

$$H_{\mathrm{y}}^{\mathrm{n}+\frac{1}{2}} = H_{\mathrm{y}}^{\mathrm{n}-\frac{1}{2}}(i, j) + \frac{E_{\mathrm{z}}^{\mathrm{n}}\left(i+\frac{1}{2}, j\right) - E_{\mathrm{z}}^{\mathrm{n}}\left(i-\frac{1}{2}, j\right)}{\Delta y}\frac{\Delta t}{\mu} \tag{5}$$

where the index n denotes the discrete time step, induces i and j denote the discretized grid point in the x-y plane, respectively. Δt is the time increment, and Δx and Δy are the intervals between two neighboring grid points along the x and y directions, respectively. In this paper we adopt the mesh to represent structure in $\Delta x : \Delta y = 2 : 1$ and each contains 15 sub meshes. Similar equations for the H polarization can be easily obtained.

Boundary conditions here we used are the perfectly matched layer (PML) [9] and Mur's absorbing conditions [10]. The net effect of this is to create an absorbing medium (which is nonphysical) adjacent to the outer FDTD mesh boundary such that the interface between the PML and the FDTD mesh is unreflectible for all frequencies, polarizations, and angles of incidence. The FDTD time-stepping formulas are numerically stable if the following condition is satisfied,

$$\Delta t \leq \frac{1}{c\sqrt{\Delta x^{-2} + \Delta y^{-2}}}$$

where c is the speed of light. In additional, the absorption in the PML's should increase quite gradually toward the outside, in order to preserve the interaction between neighboring crystal pillars or holes.

We proposed a tunable photonic crystal model in which the photonic band gap can be tuned as desired by controlling parameters. The photonic crystal structure is generated by using an ensemble of squares in periodic array (8 periods). The photonic crystals examined are composed of air rods arranged on a pitch a of 300 nm, surrounded by a sandwich of sillicon ($\varepsilon = 11.56$) in silicon dioxide to confine the light in the 2D plane.

Fig. 1 shows the transmission spectra of 2D Si-air rods photonic crystal. A 60 nm diameter of the rods is taken. At this point we assume it as normal incidence (the incidence vector $K_{\mathrm{x}} = 0$ and $K_{\mathrm{y}} = 0$) and subsequently the finite differencing mesh is applied to the structure. As is shown in this figure, the normalized frequencies at the center of the primary photonic bandgap ω_0 for TM and TE polarized waves are 0.3795 and 0.5335 fa/c. This can be directly compared with second complete PBG residing at 0.741 and 0.614 fa/c. The gap-midgap ratio ($\Delta\omega/\omega_0$) for the TE modes is

0022–2461

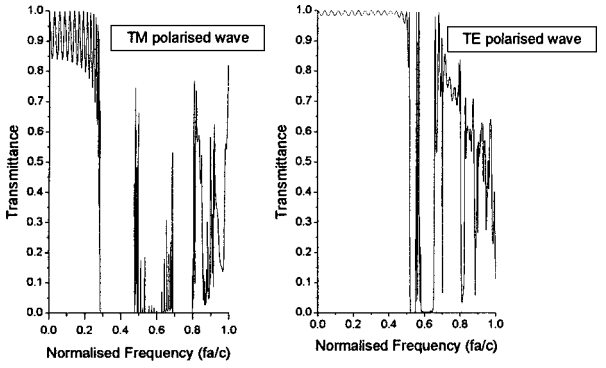

Figure 1 Transmission spectra of Si-air photonic crystal for normal incidence. Two polarized waves in TM mode and TE mode are shown.

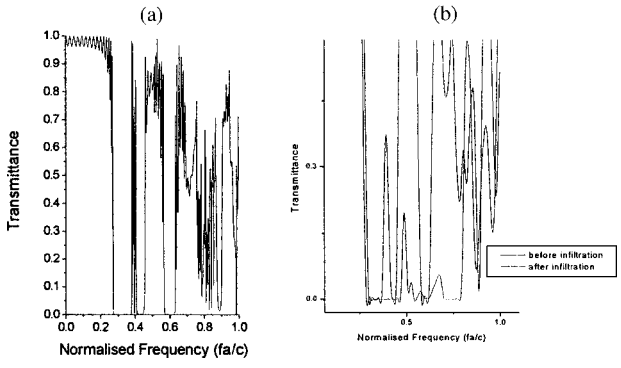

Figure 2 Transmittance spectrum of ZLI1132/Si PBG at room temperature (a). The varieties of the width of band gap are also showed (b).

5.8% and 11.2% at two bandgaps, while that of the TM modes is 51.4% and 15.7%. This gives rise to no overlap in the complete PBG for two different polarization states as a support to no complete and absolute PBG for triangular and hexagonal lattice structures for the same air filling fraction [12].

The microstructure PCs were infiltrated with nematic liquid crystal ZLI1132. The eutectic mixture ZLI1132, which is in the nematic phase at room temperature and undergoes a phase transition to the isotropic phase at 71 °C, was chosen for its acute mutation near the phase transition point. The temperature dependence of the refractive index of ZLI1132 can be found in Fig. 4 in reference [5].

With decreasing temperature, a stepwise increase of the refractive index was observed at the phase transition point between the isotropic and nematic phases. The refractive index, $n_{\text{ave}} = [(n_{\text{e}}^2 + n_{\text{o}}^2)/3]^{1/2}$ in the nematic phase is an average value of the refractive indexes for the ordinary and extraordinary lights in nematic phase, where the averaging is dependent on the director alignment, the field amplitude, and the polarization. The magnitude of the step of the refractive index was about 0.012. This is expected for an isotropic distribution in the limit where the LC-silica refractive index difference is sufficiently small that there is only weak spatial inhomogeneity of the optical electric field in the LC/Si square lattice.

In order to investigate the magnitude and direction of the observed band edge shift, calculations of the band structure of the infiltrated photonic crystal were performed using the FDTD method. The refractive index for the H-polarized field depends on the alignment of the liquid crystal director field inside the pores. The model is simplified to an axial alignment, in which the liquid crystal director is parallel to the pore axis.

Fig. 2a shows the TM transmission spectrum of LC/PCs. From 2b we can see there is a distinct stop band from 2.7–3.7 fa/c in normalized frequency, the bandgaps become narrow when liquid crystal infiltrated, and all transmission peaks go red-shift.

Because the average refractive index of LC changes little, one observed that the band edge is shift slightly in the nematic range at different temperatures. To be clearly observed, in this case, calculations of three points—30 °C, 70 °C, 71.5 °C were made and the refractive index of silicon was taken unchangeable at

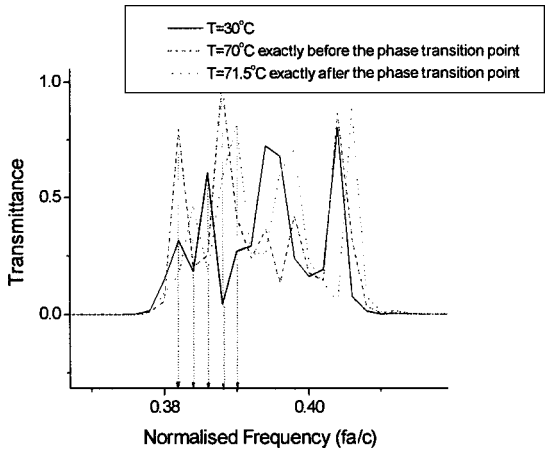

Figure 3 Transmittance spectra of LC/PGB material at different temperature.

3.400 at all temperatures. In the range the span of refractive index Δn is relatively large and the phase transition point of ZLI1132 is about 71 °C. Fig. 3 is a part of the transmission spectra. From the data of the figure we can see all the peaks go up-conversion in frequency with temperature arising. It is can be applied to whole spectra. At the same time, the band gap of LC/PCs becomes wider. As the temperature reaches the phase transition point, the LC turns into isotropic medium. The refractive index does not change any longer and so does the bandgap.

Further simulations were undertaken to highlight bandgap under the influence of filling fraction. We assume the composite PBG material has a pitch $a =$ 300 nm and LC refractive index $n_{\text{ave}} = 1.54$. The radius r of LC cylinder chooses different values, corresponding to the fraction. The curves in Fig. 4 show the normal incidence light transmit through such a structure that has a thickness of 8a, different r/a values and infinite transverse dimension.

It can be found that the widths of band gap depend on the r/a, that is to say, the filling fraction. When r/a in the range from 0.1 to 0.3, there a clear stop band in the LC/Si composite and always has three wide complete bandgaps; with the increasing ratio of r/a, the big band gaps split into many narrow gaps, the perfect photonic band gap is destroyed; on the other hand, as the ratio diminishes, the gap narrows. The numbers of gap remain unalterable but the transmission peaks boost up and the photonic band gaps vanish at last.

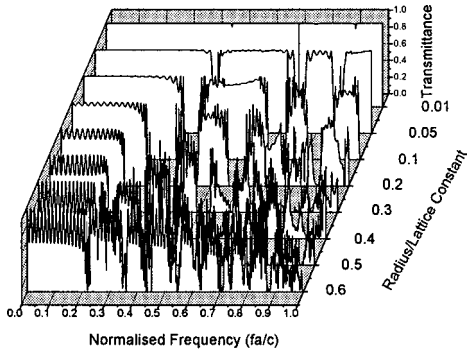

Figure 4 varieties of the band gap width in Si-LC photonic crystal.

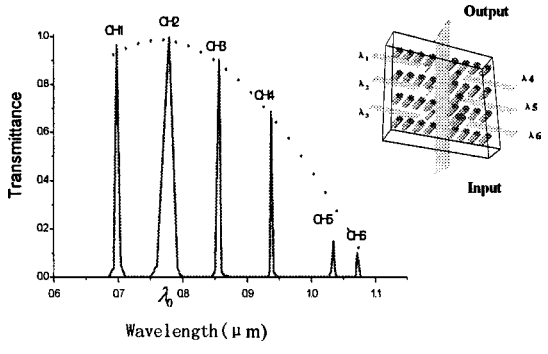

Figure 5 Wavelength spectrum of the pulses measured at each of the detectors placed inside each of the different channels of the device. For point defects, $r_1 = 15$ nm, $r_2 = 30$ nm, $r_3 = 60$ nm, $r_4 = 90$ nm, $r_5 = 120$ nm and $r_6 = 150$ nm and the corresponding wavelengths are $\lambda_1 = 0.698$ μm, $\lambda_2 = 0.779$ μm, $\lambda_3 = 0.857$ μm, $\lambda_4 = 0.937$ μm and $\lambda_5 = 1.035$ μm, $\lambda_6 = 1.071$ μm respectively.

We expanded the results to a multichannel wavelength division multiplexing (WDM) system [11, 12]. As shown in reference [11], the system included six cavities, each having a different defect size and its own guiding channel. Each channel is branched from the main waveguide.

Such a topology allows for better utilization of the structure by maximization of the density of the channels within the computations region. Combining with the data in Fig. 4, we defined six cavities with different point defects ($r/a = 0.05$–0.5) while maintaining the dielectric constant of all LC point defects and background silicon constant at $\varepsilon_r = 2.37$ and $\varepsilon = 11.56$. A separate analysis for each point defect in first PBG was performed before this case, which corresponded to each central wavelengths. We simulated the structure using, again, the FDTD method. A pulse of center wavelength $\lambda_0 = 0.785$ μm and pulse width $\Delta\lambda = 0.446$ μm was transmitted through the waveguide and the excited single state inside each cavity, the frequency of which was proportional to the size of the defect. Inside each channel we again placed a detector to obtain the wavelength spectrum of the field in each channel, which is shown in Fig. 5.

Also demonstrated in Fig. 5 is the correspondence of different point defect sizes to different localized modes with different center frequencies. The central wavelength of each channel is directly proportional to the radius of the defect; in other words, as we increase the radius of the defect, we are spanning through the available bandwidth of the incident pulse. An additional remark is that there is a limitation as to how large one can increase the radius of the defect while maintaining a single mode inside the cavity. Once the size of the defect starts getting close in size to that of the lattice rods, multiple modes start to exist in cavity. Finally, the difference in the spectral linewidths between different channels is due to the difference in Q values of different cavities, which can be optimized for equally high Q values. The most important advantage is the LC inside the cavity can broadly tune the narrow spectra features characteristic of PC based WDM. Of course, the tuning could also be used to close the band gap provide that the bandgap was sufficiently small. Using electric fields to reorient the director field, we could switch the light propagation in certain channel of LC infiltrated PC devices.

In conclusion, the focus of this work is on the simulations of electromagnetic wave propagation through two-dimensional LC/PBG materials. The FDTD method with PML absorbing boundary conditions is applied to solve Maxwell's equations when an electromagnetic wave propagation through two-dimensional array of cylinders. Further study is performed to investigate the relationships between the band gaps and the ratio of radius/lattice constant. The response for transmission spectra will also be studied for the structure in which different temperatures are introduced to the material. Finally we expand our model to a new approach for achieving a high-density wavelength selective cavities for use in WDM systems.

References

1. E. YABLONOVITCH, *Phys. Rev. Lett.* **58** (1987) 2059.
2. S. JOHN, *Phys. Rev. Lett.* **58** (1987) 2486.
3. "Photonic Band Gap Materials," edited by C. M. Soukoulis (Kluwer Academic, Dordrecht, 1996).
4. K. BUSCH and D. JOHN, *Phys. Rev. Lett.* **83** (1999) 967.
5. K. YOSHINO, Y. SHIMODA, Y. KAWAGISHI, K. NAKAYAMA and M. OZAKI, *Appl. Phys. Lett.* **75** (1999) 932.
6. S. W. LEONARD, J. P. MONDIA, N. M. VAN DRIEL, O. TODER and S. JOHN, *Phys. Rev.* B **61** (2000) R2389.
7. CHUL-SIK and H. HIM*, *ibid.* **64** (2001) 085114.
8. K. S. YEE, *IEEE Trans. Antennas ProPagat.* AP-14 (1996) 302.
9. J.-P. BERRNGER, *J. Comput. Phys.* **114** (1994) 185.
10. A. TAFLOV, "Computational Electrodynamics: The Finite-Difference Time-Domain Method" (Artech House, Norwood, MA, 1995).
11. A. SHARKWAY, SHI SHOUYUAN and D. W. PRATHER, *J. App. Opt.* **40**(14) (2001) 2247.
12. M. E. ZOOROB, M. D. B. CHARLTON, G. J. PARKER, J. J. BAUMBERG and M. C. NETTI, *Mater. Sci. Engin.* B **74** (2000) 168.

Received 29 May
and accepted 14 August 2003